AIP | Journal of Applied Physics

Secondary phase Cu2SnSe3 vs. kesterite Cu2ZnSnSe4: Similarities and differences in lattice vibration modes

Narjes Beigom Mortazavi Amiri and Andrei Postnikov

Citation: J. Appl. Phys. **112**, 033719 (2012); doi: 10.1063/1.4745894
View online: http://dx.doi.org/10.1063/1.4745894
View Table of Contents: http://jap.aip.org/resource/1/JAPIAU/v112/i3
Published by the American Institute of Physics.

Secondary phase Cu_2SnSe_3 vs. kesterite $Cu_2ZnSnSe_4$: Similarities and differences in lattice vibration modes

Narjes Beigom Mortazavi Amiri and Andrei Postnikov[a)]
LCP-A2MC, Institute Jean Barriol, Université de Lorraine, 1 Bd Arago, F-57078 Metz, France

(Received 15 May 2012; accepted 17 July 2012; published online 14 August 2012)

The crystal structure of monoclinic semiconductor Cu_2SnSe_3 is optimized, in a first-principles local density approximation calculation by Siesta method, to be found in good agreement with available experimental data, on which base zone-center transversal phonon modes are further calculated. The comparison with a similar calculation for kesterite-phase $Cu_2ZnSnSe_4$ helps to identify vibration modes promising to serve as fingerprints for discrimination of these two materials from their lattice-dynamical properties. Moreover, a full analysis of vibration modes is done, which emphasizes an importance of structural motives present in Cu_2SnSe_3 but absent in kesterite, namely continuous planar chains and stripes of like cations/anions, for the manifestation of structure-specific vibration lines. © *2012 American Institute of Physics*. [http://dx.doi.org/10.1063/1.4745894]

I. INTRODUCTION

In increasingly numerous studies being done on quaternary semiconductor systems promising for photovoltaic applications, kesterite-type Cu_2ZnSnX_4 (X = S, Se),[1–3] a "secondary phase" Cu_2SnX_3 gains importance[4] as a not always welcome, but annoyingly robust, member of the quaternary phase diagram.[5,6] It would be good to reliably identify, and separate, it from other phases, as this contamination may deteriorate the photovoltaic properties of synthesized materials. The difficulty is that the secondary phase (Cu_2SnSe_3, or CTSe for the following) has the same underlying zinc-blende structure (when neglecting the difference between cations) as kesterite or stannite phases of $Cu_2ZnSnSe_4$ (CZTSe), hence the x-ray diffraction identification is very problematic. Fortunately, the corresponding vibration spectra seem to show pronounced differences. The difficulty here is that good benchmarks which would help to pinpoint one or another phase are not yet established as such, exactly because of the difficulty to prepare, and characterize, them in a well controlled way. It should be noted that much activity in preparation of photovoltaically interesting samples occurs in thin films and not in massive bulk, so that typical problems of growth and quality control do add to the difficulty of keeping the CTSe and CZTSe phases apart.

In this perspective, we hope that first-principles calculations, relying on unambiguous structure information, may help to pinpoint such benchmarks in phonon spectra. However, our interest is of more than purely applied character. Given the overall closeness in chemistry and a tricky structural relation between the two phases, we can trace how the features of different spatial confinement emerge and give rise to different vibration motives. This may be didactically interesting, pay homage to "percolation" view on the vibration modes in semiconductor alloys[7,8] (CTSe being a nice non-trivial natural benchmark of an ordered alloy), and have impact on manipulating semiconductor superstructures.

The paper is organized as follows. Section II briefly outlines structural relations between kesterite and the secondary phase, more details of which are put into the Appendix. Section III refers to the technical side of calculations. Section IV specifies the optimized crystal structure in comparison with experiment. The main Sec. V present the discussion of vibration features mode by mode, making reference to their counterparts in kesterite and—whenever possible—to experiments, suggesting tentative attribution of the most pronounced measured modes.

II. STRUCTURAL RELATION BETWEEN PHASES

The crystal structure of CTSe, as reported by Marcano *et al.*[9,10] and refined by Delgado *et al.*,[11] is monoclinic with the *Cc* space group. In fact, its unit cell is a supercell of underlying zincblende structure, where two atom species occupy cationic sites in an ordered way (Cu being in two inequivalent positions), with $Z = 4$, hence 12 cationic sites per unit cell. Kesterite is a different ordered superstructure on the basis of zincblende, with three different cations and 8 cationic sites. The two structures are commensurate, so that doubled unit cell of CTSe matches tripled unit cell of kesterite (not stannite!) CZTSe.

The orientation of the monoclinic structure of CTSe with respect to underlying cubic is shown in Fig. 1 of Ref. 10. Two vectors of the monoclinic basal plane, **a** and **c**, go as $(\frac{1}{2}\ \frac{1}{2}\ \pm 1)$ and are thus valid translation vectors of kesterite. The **b** vector is in the basal plane of kesterite, $(\frac{3}{2}\ -\frac{3}{2}\ 0)$, which, if starting from a Cu atom in the Cu-Sn plane, would end at Sn. Therefore, this vector must be doubled in order to get a structure comprising an integer number (3) of kesterite unit cells. More precisely the transformation of basis vectors is described in Appendix. We only emphasize here, as was also stated by Delgado *et al.*,[11] that copper atoms have two inequivalent positions, whereby selenium has three. The nearest neighborhoods of anions are (Cu1, Cu2, 2 × Sn) to Se1, (Cu1, 2 × Cu2, Sn) to Se2, (2 × Cu1, Cu2, Sn) to Se3,

a)Electronic mail: andrei.postnikov@univ-lorraine.fr.

and (of cations) (Se1, Se2, 2 × Se3) to Cu1, (Se1, 2 × Se2, Se3) to Cu2, (2 × Se1, Se2, Se3) to Sn. The explicit numbering and positioning of atoms is given in the Appendix.

III. CALCULATION ASPECTS

The present calculations have been done from first principles, at the accuracy level provided by the density functional theory, specifically, the local density approximation (LDA), using the Siesta method and calculation code.[12–14] Norm-conserving pseudopotentials constructed with the Troullier-Martins scheme[15] were used in combination with atom-centered strictly confined localized basis functions. The calculation setup is identical to that used in Ref. 16. The calculations on the kesterite phase have not been re-done here, as compared to this publication, but we bring to attention some further vibration modes than previously discussed, for the sake of the present comparison.

An obvious shortcoming of our calculation is the underestimation of the band gap and, as a consequence, a very limited usefulness for discussing electronic properties. However, it has been shown on many occasions that ground state-related results, such as equilibrium geometry, forces on atoms and hence phonons, are quite reliable, so that more sophisticated hybrid-functional or GW calculations are not (yet) prerequisite of a reliable lattice-dynamics study. As concerns the electronic structure with the accent on optical properties, the necessary information was provided by a recent work by Zhai *et al.*,[17] who did a hybrid-functional calculation for monoclinic CTSe, among other ternary structures.

Another limitation, that we only discuss the zone-center vibration modes, is of purely technical character and could have been overcome in our calculation approach. However, for discussing a possible impact on Raman or infrared spectra, only zone-center vibrations are of interest anyway. Moreover, having already a quite large unit cell of the CTSe phase and hence correspondingly reduced Brillouin zone, discussing dispersions of its many phonon branches would not obviously contribute any clearness to the present analysis. And finally, having different unit cells of CZTSe-kesterite and CTSe, an attribution of their relative phonon dispersions would be not straightforward. At Γ, such comparison is easier.

IV. STRUCTURE OPTIMIZATION

The internal coordinates of atoms in monoclinic CTSe were given by Delgado *et al.*[11] The details on the crystal structure and its relation to kesterite are explained in the Appendix; for the present it suffices to know that the underlying lattice is a very little distorted zincblende, over cationic sites of which the Cu and Sn atoms are ordered.

In the course of relaxation, even as no symmetry constraints have been imposed on the lattice, the latter remained well monoclinic [α and γ stay at $(90\pm10^{-4})^\circ$], yielding lattice parameters $a=6.939$ Å, $b=11.950$ Å, $c=6.975$ Å, $\beta=109.72^\circ$ and unit cell volume $V=544.45$ Å^3. These can be compared with experimental data of Ref. 11, $a=6.967$ Å, $b=12.049$ Å, $c=6.945$ Å, $\beta=109.19^\circ$, $V=550.6$ Å^3 (a and c apparently being inversed, compared to our setting). The underestimation of lattice parameters in LDA is typical; the present error (1%, for the volume) is in fact unusually small. We note however that earlier experimental data by Marcano *et al.* ($a=6.5936$ Å, $b=12.1593$ Å, $c=6.6084$ Å, $\beta=108.56^\circ$)[9,10] are rather at variance with both Delgado's results and our present ones.

An attribution of different sites with their respective coordinates, as extracted from x-ray diffraction, is given in Table III of Ref. 11. As the Siesta calculation does not impose symmetry constraints, the coordinates of all 24 atoms are independently adjusted, along with lattice parameters, in the course of relaxation. In order to facilitate the comparison with experiment, the nominal fractional coordinates within each group of (four) atoms are averaged, upon applying symmetry transformations between corresponding Wyckoff positions; the results are given in Table I.

The resulting bond lengths are summarized in Fig. 1. On top of fairly good overall agreement, one can note that Sn–Se bonds are systematically overestimated in calculation, at the expense of reduced Cu–Se ones. Put differently, the Se1 and Se2 atoms are off-centered in their respective cation tetrahedra more versus Cu and away from Sn than they should (Table II).

V. DISCUSSION ON PHONONS

The zone-center frozen phonon calculation on CTSe yields 3 (acoustic, zero-frequency) + 69 further modes, which, atomic differences within the each sublattice neglected, would map a number of optical-like and acoustical-like vibrations at some $\mathbf{q}$ values of the underlying zincblende lattice. Of primary practical interest is a comparison with Raman and infrared spectra, probing $\mathbf{q}=0$ vibrations. Unable to strictly calculate corresponding intensities, we use the technique of projection of phonon eigenvectors onto a vibration pattern corresponding to a given $\mathbf{q}$ (see Eq. (1) of Ref. 16), notably $\mathbf{q}=0$ in the present case. This strictly suppresses vibration which involve atoms of

TABLE I. Internal coordinates in CTSe as presently calculated and reported in Ref. 11 (all in 4*a* Wyckoff positions of the *Cc* space group). The calculated values are averages over four nominally equivalent positions within each type; see text for details.

Type	*x*	*y*	*z*
		Calculation	
Cu1	0.3864	0.2535	0.6206
Cu2	0.3983	0.4175	0.1206
Sn	0.3772	0.0914	0.1015
Se1	0.0344	0.4023	0.0090
Se2	−0.0207	0.0838	−0.0209
Se3	0.5261	0.2660	−0.0203
		Experiment	
Cu1	0.371(3)	0.257(1)	0.616(3)
Cu2	0.370(3)	0.418(1)	0.116(3)
Sn	0.363(3)	0.091(1)	0.107(3)
Se1	0.000	0.409(1)	0.000
Se2	−0.026(3)	0.078(1)	−0.015(3)
Se3	0.503(3)	0.259(1)	−0.014(3)

TABLE II. Bond lengths in CTSe according to present calculation and x-ray diffraction data of Ref. 11.

	Cu1	Cu2	Sn
	Calculation		
Se1	2.380	2.384	2.679
Se2	2.366	2.370	2.602
Se3	2.367	2.370	2.595
	Experiment		
Se1	2.44(2)	2.44(2)	2.59(2)
Se2	2.39(2)	2.38(7)	2.57(3)
Se3	2.43(3)	2.43(3)	2.51(2)

the same species in counterphase. The rest of analysis, e.g., identification of "optical-like" modes in which cation vibrate against anions rather than in phase, has to be done by immediate inspection.

Fig. 2 compares the vibration density of states, calculated along Eq. (1) of Ref. 16 with $\mathbf{q} = 0$, for kesterite structure of CZTSe and for CTSe. The upper panel in fact depicts the system of modes earlier published in Fig. 5 (middle panel) of Ref. 16, but now plotted with better resolution (broadening halfwidth of $2\,\mathrm{cm}^{-1}$). The character of each mode is explained in Table I of Ref. 16.

Observing the overall similarity in the placement of three separated dense groups of vibration lines ($50-90\,\mathrm{cm}^{-1}$, $140-190\,\mathrm{cm}^{-1}$, and $200-250\,\mathrm{cm}^{-1}$, that equally applies to CZTSe stannite and $CuInSe_2$ chalcopyrite, see Ref. 16), we note, as the most striking difference, that in CTSe the second group is broader and gets softened. Two other groups roughly maintain their widths as in kesterite, exhibiting however a slight red shift, and their composition (in what concerns the involvement of different atoms in vibrations) is sometimes different. We note in passing that the counting of modes within each group is conform between kesterite and CTSe: having a tripled number of atoms and hence of zone-center modes in the latter phase, e.g., the modes 10 through 13 of kesterite are "replaced" by modes 30 through 39 in CTSe.

Given a moderate number of atoms in the primitive cells and a fair amount of residual symmetry in corresponding phases, non-negligible symmetric patterns can be found in, at least, some phonon modes of kesterite (easy to see) and of CTSe (somehow hidden). The intricacy of such comparison is that symmetry patterns of tetragonal kesterite (displacements parallel to edges, or basal diagonal) are replaced to symmetry of "almost hexagonal" planes, "hidden" in the CTSe structure. In the following, we briefly discuss the nature of some vibration modes responsible for the pronounced, or otherwise interesting, peaks in the zone-center density of modes shown in Fig. 2.

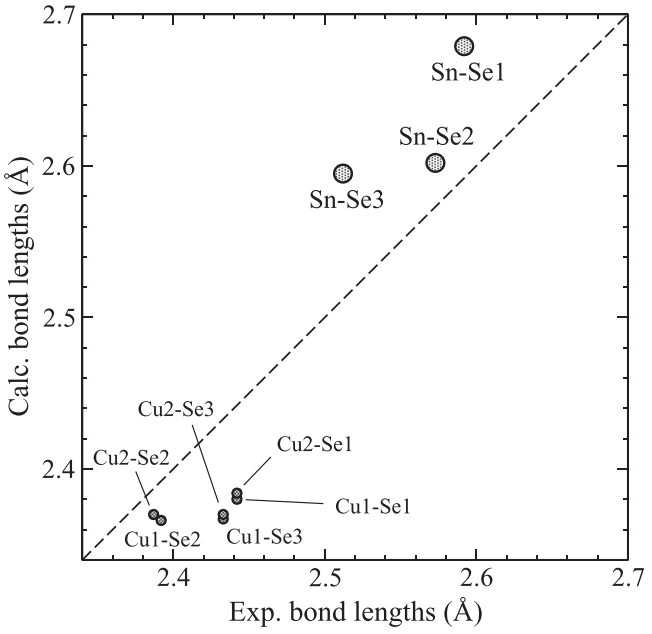

FIG. 1. First-neighbor interatomic distances from calculated structure relaxation in comparison with experimental data of Ref. 11.

A. The softest modes (50–90 cm^{-1})

The vibrations within this lower group are, basically, zone-boundary acoustic modes of the zincblende aristotype; their non-zero projection is only due to the non-equivalence of cations, whereas the contributions from Se do largely cancel out. In these modes, cations tend to move in phase with, at least, some neighboring anions; such "acoustic" movements of certain groups of atoms occur in opposite phase to the other ones. In the mode #12 ($59.8\,\mathrm{cm}^{-1}$), the -Cu1-Se3-Cu1-Se3- chains transversing the crystal along [101] do rigidly move parallel to their own direction, against the

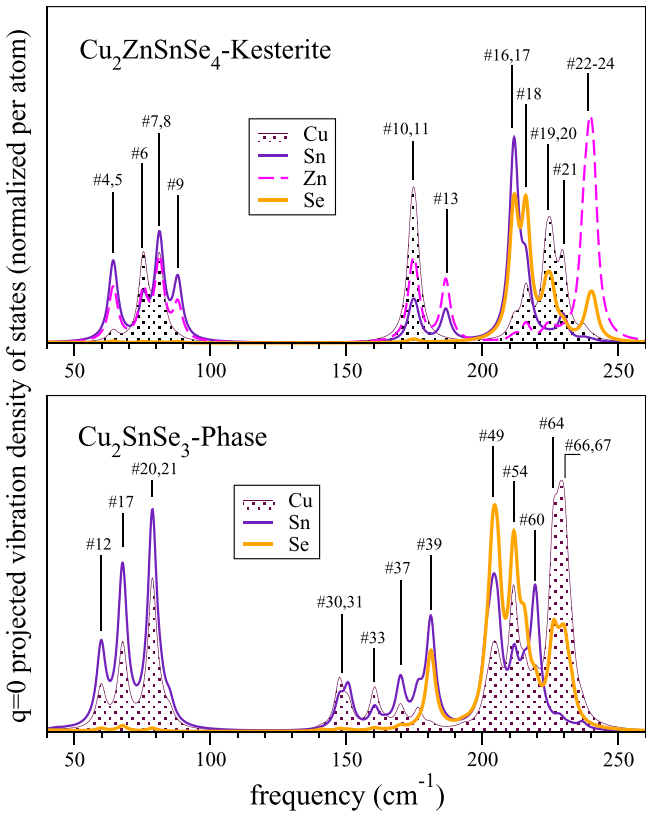

FIG. 2. Calculated zone-center density of modes in CZTSe-kesterite (top panel, from Ref. 16) and CTSe (bottom panel, present calculation). Some modes in throughout numbering are indicated, for reference in the text.

(Cu2+Sn+Se1+Se2) bulk. In the mode #13 (60.1 cm^{-1}), two adjacent (010) planes that make such (Cu2+Sn +Se1+Se2) "layer" (see details of structure in Appendix) undergo rigid (in-plane) movement in the opposite sense, whereas the third interlacing ($2 \times$ Cu1 $+ 2 \times$ Se3) plane, containing the previously mentioned chains, does not move. As a result, this mode yields zero contribution to the $\mathbf{q} = 0$-projected density of modes. The mode #17 at 67.7 cm^{-1} involves almost perfectly planar movement, somehow scattered within the (010) planes around the general [001] direction, of Sn with Se1, roughly, in one sense, and of Cu2 with Se2—in the opposite one, Cu1 and Se3 being, again, not much involved.

As frequencies increase within this group of lines, the folding of the zone-boundary modes becomes less evident; the nearest cations and anions gradually go out of phase, developing a "more optical" character of modes. The mode #20 (78.6 cm^{-1}) still retains the tendencies of neighboring cations and anions to move together and not produce much stretching; however, their displacements at almost right angle are common, and the resulting pattern of bond bendings becomes quite rich. The vibrations in the mode #20 are essentially confined to (001) planes of the monoclinic CTSe structure, shown in the view of the crystal lattice along [010] in the top left panel in Fig. 3. The definition of monoclinic lattice vectors given in the Appendix makes apparent that such planes are (111) ones of the underlying zincblende aristotype (the difference between cations being neglected), piled as warped double-layers of cation-anion honeycomb network. Each double-layer maintains the stoichiometry of the compound, having all six inequivalent atoms to appear along the perimeter of each hexagon. The presence of a tin atom at one vertex distorts somehow the "hexagonality" within these planes of the relaxed structure. However, the vibration pattern within each plane is nicely symmetric: out of three hexagons per unit cell in the plane, one flips back and forth between two trigonal distortions, while the others around it make a roughly rigid rotational movement. The vibrations within both layers are of course identical, however, with trigonal distortion (cations inwards/anions outwards) being in opposite phase, and vibration pattern as a whole being in-plane displaced and rotated. The mode #21, degenerate with the present one, looks identical, only that, the displacement vector on each individual atom being rotated by 90°, a previously "deforming" hexagon becomes a "rigid rotating" one, and vice versa. The resulting movement of all Se atoms sums up to almost zero and hence disappears in the density of modes in Fig. 2, whereas the resulting movement of Sn over both planes is large, and points opposite to that of Cu. Even if this looks like an overall Sn vs. Cu mode, the Cu–Se and Sn–Se bonds in the deformed hexagons undergo a strong bending, so that the prominence of this mode in the resulting spectrum might be important.

From the frequency and composition of modes #20,21 in CTSe, their "natural counterparts" in the kesterite CZTSe seem to be the modes #7,8. However, a careful inspection of the vibration patters in the latter gives no hint of their confinement to the zincblende (111) planes—or, equivalently, the (112) planes of the kesterite structure. Similarly, no "hexagon dance" becomes apparent in these modes of kesterite, whereas their attribution to the axes of the tetragonal cell, and the

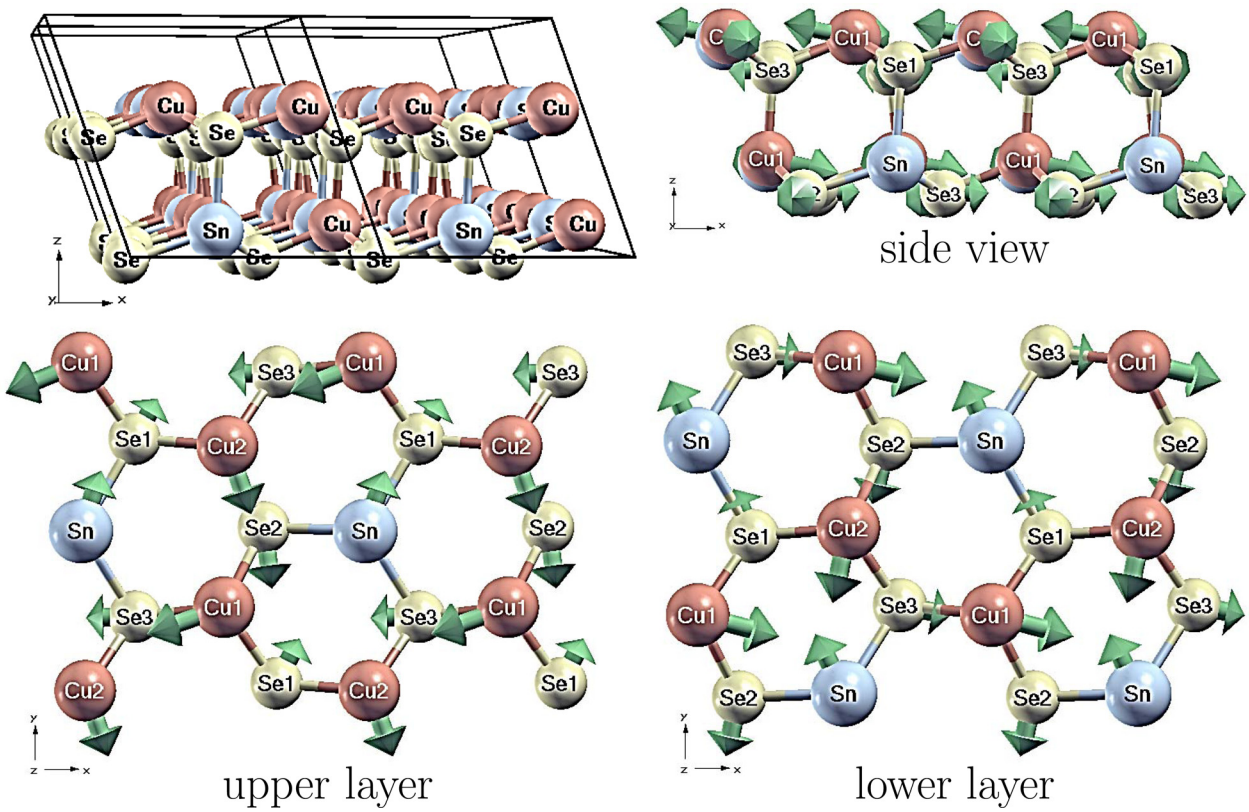

FIG. 3. Snapshot of the vibration mode #20 at 79 cm^{-1} in two adjacent (001) hexagonal layers (Se1 of the upper layer docked on top of Sn in the lower layer) and in the side view along [010]. The placement of layers in the unit cell is shown in the upper left panel.

corresponding nature of their degeneracy, as was previously discussed in Ref. 16, are unambiguously pronounced.

B. Intermediate modes (140−190 cm^{-1})

Here, we enter the range of "genuine" optical modes. The gradual increase of intensity in the $\mathbf{q} = 0$ -projected density of modes towards the upper end of the spectrum reveals that the "all cations vs. all anions" character becomes more prominent with frequency. A typical motif of vibration is cation vs. anion movement at an angle to their connecting bond, i.e., vibrations are of markedly bond-bending type. Somehow simplifying, one can note that the displacement-to-bond angle gradually decreases as frequency grows throughout the 140 → 190 cm^{-1}, so that the upper vibration modes are already quite in the bond-stretching regime.

The softest in this group, the mode #30 (147.4 cm^{-1}) is confined within the -Cu2-Se2-Cu2-Se2- stripe, a zigzag chain slightly warped around the (100) plane and running along [001] of the monoclinic structure. The edges of such stripes are formed by the -Cu1-Se3-Cu1-Se3- chains, which are knitted together into the purely Cu1,Se3 (010) planes. The cross-sections of such stripes are outlined in Fig. 4(a) by green ovals. The edge Cu1-Se3 atoms vibrate only weakly, the atoms along each given [001] line being in phase (see Fig. 4(b)), but in alternating sense from one stripe to the neighboring one—a relict of acoustic zone-boundary behavior. On the contrary, the inner Cu2 and Se2 atoms vibrate "optically" and in "zone-center way," all Cu2 in phase throughout the crystal against all Se2, that bends the bonds within the stripe. The mode #31 (149.0 cm^{-1}) differs in that the sense of Cu2, Se2 vibrations alternates in consecutive (100) planes; moreover the magnitude of Se2 displacements reduces considerably, and the stripe-edge atoms, Cu1 and Se3, vibrate yet weakly but now in opposite to each other. Due to general inversion of all displacements when passing from one (100) plane to the next chemically identical one, the net zone-center projection of this mode yields zero. The mode #32 (150.7 cm^{-1}) roughly

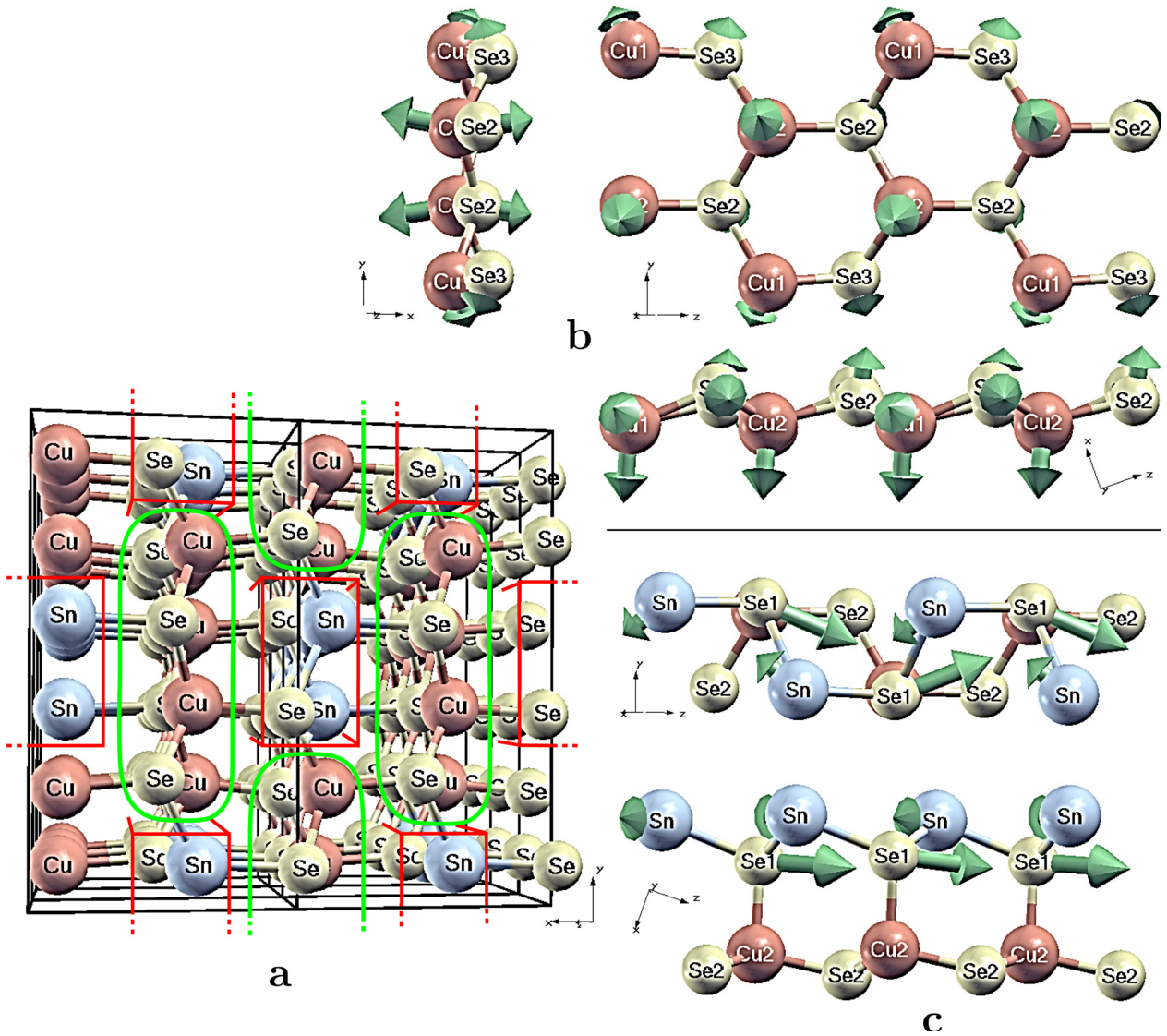

FIG. 4. (a) Crystal structure of CTSe, viewed along [001]. Isolated -Sn-Se1-Sn-Se1- stripes, along which the mode #39 propagates (perpendicular to the plane of figure), are outlined by red boxes. -Cu2-Se2-Cu2-Se2- stripes bordered by -Cu1-Se3-Cu1-Se3- chains, running in the same direction, which are relevant for the mode #30, are outlined by green ovals. (b) Snapshot of the vibration mode #30 at 147 cm^{-1} with Cu1 and Se2 vibrating perpendicular to "their" stripe, shown in three projections. (c) Snapshot of the vibration mode #39 at 181 cm^{-1} with Sn and Se1 vibrating along "their" stripe, shown in two projections.

retains the same system of stripes and out-of-plane vibrations, but now the displacements of consecutive Cu2 *along the stripe* occur in opposite, the vibration of in-between Se2 disappears, whereas Cu1 develop a net (in-phase) component of vibration out of (010) Cu1,Se3-planes. Se2 and Se3 do not participate much in this mode, whereas the Se1 are involved in a (largely acoustic—zone-boundary) interplay with Sn. The mode #33 (160.2 cm^{-1}) is difficult to make sense of; in any case, a transparent system of stripes and either in-phase or plane-by-plane alternate vibration motives is gone, without being replaced by any new emerging clear symmetry.

Such different symmetry reappears in the mode #37 (169.9 cm^{-1}) which is roughly planar in the (001) plane, as was mode #20 (Fig. 3). More precisely, the atoms tend to move slightly upwards or downwards from these planes, along the bonds to their neighbors in the warped hexagonal layers.

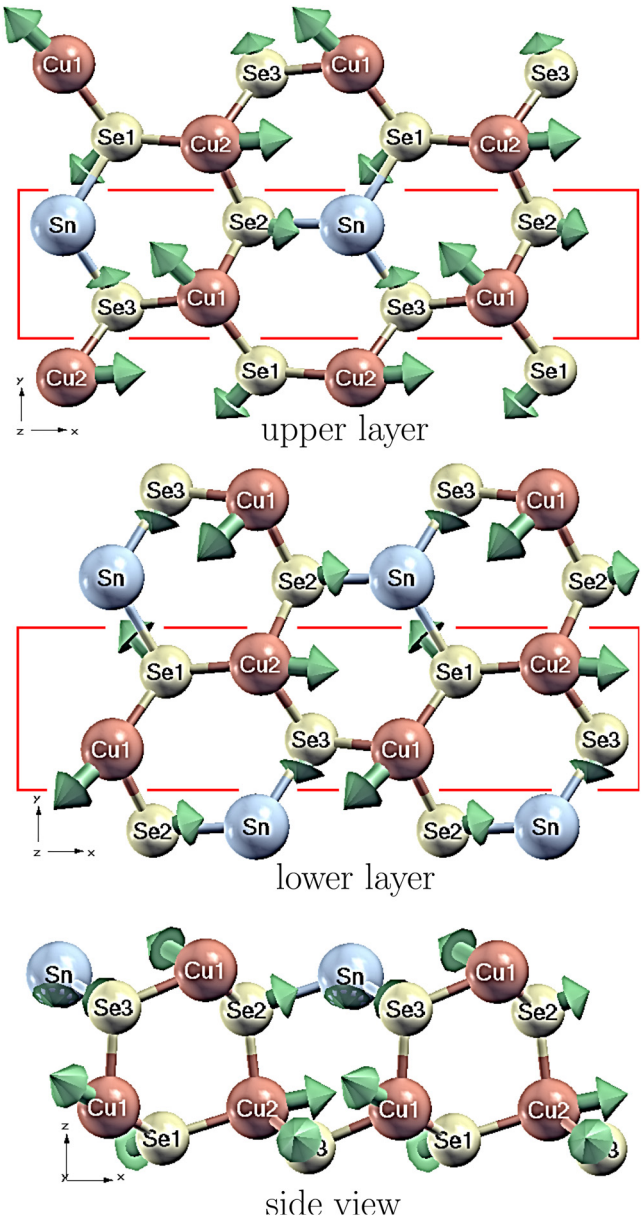

FIG. 5. Snapshot of the vibration mode #37 at 170 cm^{-1} in two adjacent (001) hexagonal layers and in the side view along [010], the setting similar to that of Fig. 3. The side view shows only atoms within the box the red trace of which is shown on both layer projections.

A snapshot of this mode is shown in Fig. 5 in two adjacent planes and a side view along [010]. As previously emphasized for other modes from the middle (140–190 cm^{-1}) group, a vibration of neighboring cations against anions at some angle, leading to bond bending rather than clear stretching, remains here a marked element. However, some elements of stretching are not to overlook: first of all, a nicely symmetric "breathing" of three (different) Se anions occurs around an immobile Sn; moreover, a pair of Cu1 and Cu2 in their concerted motion stretches their bonds to Se1. Taken together, the periodic vibration pattern is such that Cu2 moves roughly parallel to its two neighboring Se2, one being in the (001) plane and the other in the adjacent plane. Tracing their further connections, we can recognize the -Cu2-Se2-Cu2-Se2- stripes already discussed above and note that the Cu2 vibrate perpendicular to the plane of these stripes, being accompanied by Se2 moving in phase. However, the vibrations in the rest of crystal are not clear in this perspective, that is why we do not show the mode #37 in the "stripe" projection like in Fig. 4.

One notes that Cu1 moves at roughly the right angle relative to its Se1 and Se2 neighbors. Another observation concerning the mode #37 is that the vibration patterns in two adjacent (001) planes are not in opposite phase, as is the case, e.g., for the mode #20 shown in Fig. 3, but in-phase. More precisely, their vibration patterns are related by (010) mirror-plane symmetry, as also are the very structures of adjacent planes—see Appendix.

For the discussion of mode #39 (181.1 cm^{-1}), we come back to Fig. 4(a) depicting the stripes running along the [001], but now concentrate on the -Sn-Se1-Sn-Se1- stripes, whose cross-sections are outlined by red boxes. Such stripes are *isolated*, i.e., completely surrounded by the (Cu1, Cu2, Se2, Se3) matrix which is out of resonance in this mode. The snapshot of this vibration (Fig. 4(b)) shows that Sn and Se atoms move in opposite, each one towards its next homologue along the stripe. For the mode #40 nearly degenerate with the latter (181.6 cm^{-1}), the displacement pattern within each stripe is almost exactly the same, however, adjacent stripes, separated on the lattice by -Cu-Se-Cu-Se- links, move in counterphase. The $\mathbf{q} = 0$-projected density, summed up over all Sn atoms, for this mode is nearly zero, but, considering that the stripes are distant and rather independent, one can expect a considerable Raman signal from this mode as well.

In fact, these modes are natural suspects for associating them with a strong Raman line observed by Altosaar *et al.*,[18] Grossberg *et al.*,[19] and Marcano *et al.*[20] at 180 cm^{-1} in CTSe. We remind that in both the experiment and our calculation, the line in question markedly falls in between two strong peaks attributed to the CZTSe kesterite (modes #10,11 at 174 cm^{-1} and #13 at 187 cm^{-1} in the upper panel of Fig. 2, tentatively attributed in Ref. 16 to measured lines at 173 and 196 cm^{-1}, e.g., in Ref. 18).

C. The hardest modes (200–240 cm^{-1})

We turn now to the third group of vibration modes, which exhibit more pronouncedly bond-stretching character. Vibrations in the mode #49 (203.8 cm^{-1}) are confined to (001) planes of the monoclinic CTSe structure (already

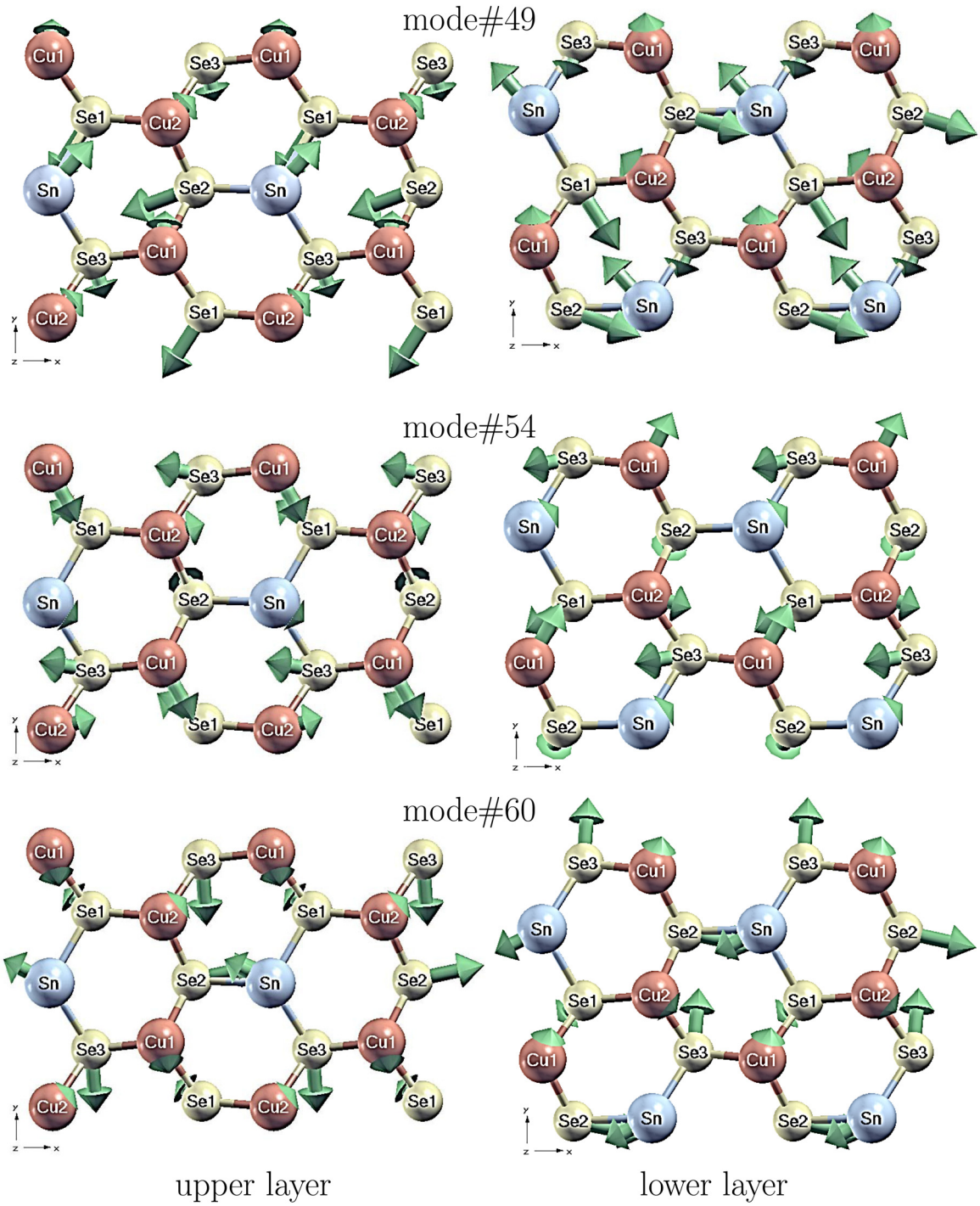

FIG. 6. Schematic snapshots of the vibration modes #49 (at 204 cm^{-1}, upper row), #54 (at 212 cm^{-1}, middle row), and #60 (at 219 cm^{-1}, bottom row) depicting the atoms in two consecutive warped (001) planes (left/right column), similar to those shown in Fig. 3.

discussed above in relation with the modes #20 and #37) to the extent roughly similar to that shown in the "side view" projection of mode #20 in Fig. 3. The in-plane vibration pattern in two adjacent planes is shown in the upper row of Fig. 6, for the in-plane fragments identical to those depicted in Fig. 3; we recall that Se1 of the upper layer resides on top of Sn from the lower layer. The key feature of the #49 vibration mode is the stretching of the Sn–Se1 bond, which would mark the mirror plane in an isolated warped layer. At the same time, Se2 and Se3, which move at right angle one to the other, produce a "resulting motion" roughly parallel to that of Se1 and, hence, against the Sn. One out of three hexagons in the planar unit cell gets "rectangularly" deformed along its Sn–Se1 main diagonal; the neighbors on both sides of this plane adjust to this movement, and two other hexagons suffer a complicated deformation. Since the main Sn–Se1 axes in two adjacent planes stand at (approximately) 120° to each other, the above mirror symmetry in each layer is not perfect. Moreover, the axial compressions/dilations of the "symmetric" hexagon go interchanged layer by layer. In total, this vibration mode offers a rich pattern of stretchings and bendings of cation–anion bonds; moreover, it reveals a clear

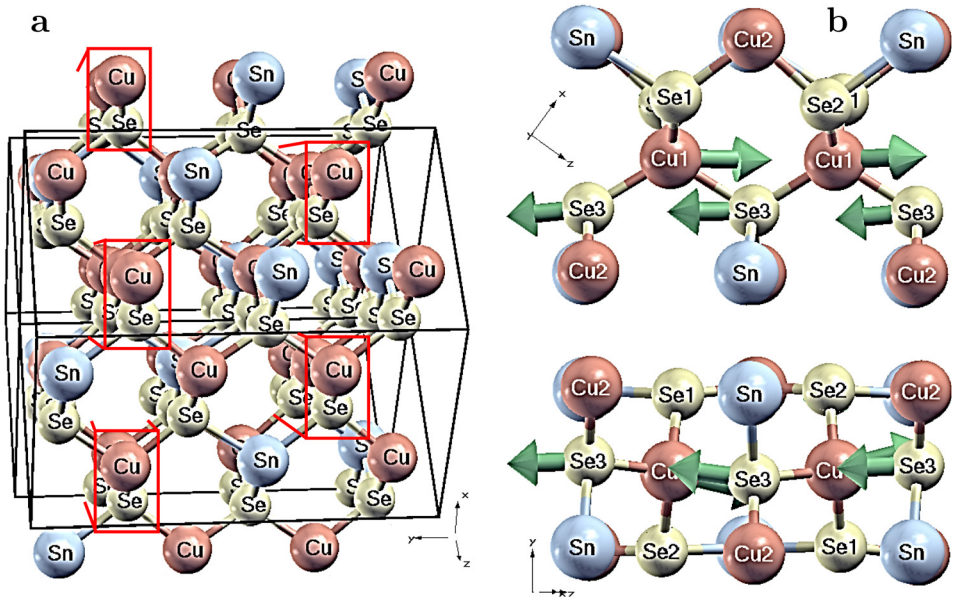

FIG. 7. (a) Crystal structure of CTSe, with isolated -Cu1-Se3-Cu1-Se3- chains running along [101] (perpendicular to the plane of figure) outlined by red boxes. (b) Snapshot of the vibration mode #66 at 230 cm^{-1} shown in two projections.

combined movement of Se atoms against *both* Cu and Sn. The resulting vector of the cation–anion separation (i.e., the varying net dipole moment) goes along [010]. This mode does not have obvious counterparts in CZTSe-kesterite, and it seems to be important one for spectroscopic identification of the CTSe phase, capable to yield a big spectral signal.

Vibrations in the mode #54 (211.7 cm^{-1}) do also occur essentially in the (001) plane; the (almost) in-plane atomic displacement patterns are shown in Fig. 6, middle row. The principal stretching in this mode is that of the Cu1–Se1 bonds, accompanied by an asymmetric distortion of the neighboring hexagons. When coming from plane to plane, the direction of this stretching bond turns again (in alternation) by about 120° back and forth. In fact, one notices the cations-vs.-anions movement along "heterogeneous" stripes -Cu2–Se3–Cu1–Se1–Cu2- which run in the [100] direction (e.g., two such chains flank the horizontal edges of the fragment cut in Fig. 6 for the upper layer). Sn and Se2 atoms sitting on the middle line between such stripes are not much affected by the vibration, but still, the net movement of Sn is in the same sense as other cations, that is, along [100], perpendicularly to the dipole moment variation in mode #49.

These two modes seem to be two manifestations of the generic "all-cations-against-all-anions" Γ-TO mode, triply degenerate in zincblende structure but having the degeneracy lifted as the symmetry is reduced. In the kesterite phase, the related mode was #18 at 216 cm^{-1}, singled out because of tetragonal symmetry.

The mode #60 (219.4 cm^{-1}) does, in a sense, "complement" the mode #49 vibration, in that Sn, now *in phase* with Se1, moves roughly *against* the resulting motion of Se2 and Se3, these two being again, as in the mode #49, at right angle one to the other. Interestingly, one can find similarities with mode #20 if reversing the movement of all cations (or all anions): whereas there we saw a "rotation" of hexagons due to neighboring cations and anions moving in phase, now we find "benzene-like" deformation due to anions moving in opposite to cations and thus stretching the bonds in alternation along the hexagons' perimeter.

We conclude our discussion by the mode #66 (230.2 cm^{-1}) which is fully confined within the (planar) zigzag -Cu1-Se3- chains. Fig. 7(a) shows how these chains run through the crystal lattice in the [101] direction. They are separated from each other by the -Sn-Se1-Cu2-Se2- chains which are out of resonance at the frequency in question. Fig. 7(b) shows the atoms in the chain with some their neighbors, in the "side view" and the "top view" (with respect to the orientation of chains in Fig. 7(a)). It is well seen, especially in the "top view," how the chain undulates passing through the crystal. An almost degenerate mode 67 (230.5 cm^{-1}) differs from the mode 66 in that the movements within two chains transversing the unit cell occur in counter phase. We note that such planar -Cu-Se-Cu-Se- chains do not occur in the kesterite-type CZTSe, where all the chains are of mixed cation composition. The closest in nature to the "along the chain" vibration among those in kesterite are the (degenerate) modes 23 and 24 at 239 cm^{-1} (see Table I and Fig. 6 of Ref. 16). In them, however, the copper is not moving, and hence "isolated" -Se-Zn-Se- fragments vibrate at higher frequency. In the stannite-type CZTSe, on the contrary, one finds the -Cu-Se-Cu-Se chains running along the basal diagonals; two other bonds of each Se are saturated by Zn and Sn in crisscross sequence, similar to how Cu2 and Sn are attached in Fig. 7. However, no vibration mode of stannite which we have studied earlier[16] is any close to a pure along-the-chain vibration; either the movement of atoms is not quite transversal, or other out-of-chain atoms are strongly mixed in (see Table II and Fig. 7 of Ref. 16). Therefore, the mode #66 is expected to be a strong signature of the CTSe phase, neither typical to kesterite-type nor to stannite-type CZTSe. In the absence of more detailed identification based on the analysis of Raman intensities, we are tempted to identify this more with the peak at 236 cm^{-1} reported by Altosaar *et al.*[18]

The visualization of chains in Fig. 7 helps to explain the lowest mode which yields a non-negligible zone-center projection in Fig. 2, that is, mode #12, mentioned above to have basically a zone-boundary acoustic character. The -Cu1-Se3- chains outlined in Fig. 7 make, in mode#12, rigid entities

which move (along the chain direction) against the rest of crystal (interconnected -Sn-Se1-Cu2-Se2- chains). The "optical" nature of such vibration comes from the bending of side bonds to the -Cu1-Se3- chains.

VI. CONCLUSION

Summarizing, we present comparative results of frozen-phonon calculations for two chemically and structurally related ordered compounds, "secondary phase" Cu_2SnSe_3 and kesterite-type $Cu_2ZnSnSe_4$. There is similarity in positioning of three main groups of spectral lines, which we identify now, in the order of increased frequency, as manifestations of (i) mostly acoustic zone-boundary modes; (ii) mostly optical bond-bending modes, and (iii) genuinely optical bond-stretching modes, understanding all ambiguities of such attribution in case where all modes exhibit more or less mixed behavior. Moreover, the "master" TO mode (all cations against all anions) can be found at about the same frequency. However, a noticeable mismatch in frequencies and character of some lines between CZTSe and CZSe can be traced to different cation arrangements in these systems. Unexpectedly, the absence of Zn in one of compounds, even if having a limited effect on particular spectral lines, does not seem to produce such important overall differences, as does different topology of cation sublattices. The presence of chains or stripes of different composition and connectivity, along which different modes come to resonance, seems to have much larger effect. Specifically, we suggest that the modes like #30 ($147\,cm^{-1}$) and #39 ($181\,cm^{-1}$), which "live" on infinite homogenous cation-anion stripes not existing in kesterite, or mode #66 ($230\,cm^{-1}$), confined to Cu-Se chains, another unique feature of CTSe, can serve as lattice-dynamical fingerprint of this latter compound, the more so that the latter vibration line does apparently appear in measured Raman spectra.

ACKNOWLEDGMENTS

Cooperation with Susanne Siebentritt was crucial for bringing the secondary phase into our attention, in the context of related studies on kesterite-structure photovoltaic materials. We appreciate enlightening correspondence with Jüri Krustok and Maarja Grossberg, who made us aware of their unpublished results. Moreover, we are grateful to Michael Yakushev for careful reading of the manuscript and suggestions. The calculations have been done using computation resources of the PMMS at the Paul Verlaine University—Metz.

APPENDIX: LATTICE VECTORS AND ATOM SITES OF CTSE AND CZTSE IN DIFFERENT SETTINGS

Let **a**, **b**, **c** be lattice vectors of kesterite structure in conventional setting relative to underlying cubic (zincblende) lattice, say $\mathbf{a} = (1\,0\,0), \mathbf{b} = (0\,1\,0), \mathbf{c} = (\frac{1}{2}\,\frac{1}{2}\,1)$, and cation coordinates as in Table III. The monoclinic structure of CTSe is constructed on translation vectors $\mathbf{A} = (\frac{1}{2}\,\frac{1}{2}\,1) = \mathbf{c}$, $\mathbf{C} = (\frac{1}{2}\,\frac{1}{2}\,-1) = \mathbf{a} + \mathbf{b} - \mathbf{c}$; the third vector we take doubled, for commensurability with kesterite: $\mathbf{B} = (3\ -3\ 0) = 3\mathbf{a} - 3\mathbf{b}$. Therefore,

TABLE III. Cation positions in the CZTSe kesterite structure. Cartesian coordinates are in the units of a (assuming $c = 2a$), fractional coordinates are in the units of **a**, **b**, **c**.

Atom	Cartesian			Fractional		
Cu1	0	0	0	0	0	0
Cu2	0	$\frac{1}{2}$	$\frac{1}{2}$	$-\frac{1}{4}$	$\frac{1}{4}$	$\frac{1}{2}$
Sn	$\frac{1}{2}$	$\frac{1}{2}$	0	$\frac{1}{2}$	$\frac{1}{2}$	0
Zn	$\frac{1}{2}$	0	$\frac{1}{2}$	$\frac{1}{4}$	$-\frac{1}{4}$	$\frac{1}{2}$

$$\begin{pmatrix}\mathbf{A}\\ \mathbf{B}\\ \mathbf{C}\end{pmatrix} = \begin{pmatrix}0 & 0 & 1\\ 3 & -3 & 0\\ 1 & 1 & -1\end{pmatrix}\begin{pmatrix}\mathbf{a}\\ \mathbf{b}\\ \mathbf{c}\end{pmatrix}, \tag{A1}$$

$$\begin{pmatrix}\mathbf{a}\\ \mathbf{b}\\ \mathbf{c}\end{pmatrix} = \begin{pmatrix}\frac{1}{2} & \frac{1}{6} & \frac{1}{2}\\ \frac{1}{2} & -\frac{1}{6} & \frac{1}{2}\\ 1 & 0 & 0\end{pmatrix}\begin{pmatrix}\mathbf{A}\\ \mathbf{B}\\ \mathbf{C}\end{pmatrix}. \tag{A2}$$

The monoclinic angle is

$$\beta = \arccos\frac{2-(c/a)^2}{2+(c/a)^2},$$

for $c = 2\,a$, $\beta = 109.47°$, the tetrahedral bond angle. The determinant of the transformation matrix in Eq. (A1) is 6, therefore, each of the atoms in Table III has to be sextupled

TABLE IV. Cation coordinates in the CZTSe kesterite structure, expanded over the doubled monoclinic cell. Cartesian coordinates are given in units of $a/2$, fractional ones in units of **A**/2, **B**/12, **C**/2.

	Cartesian			Fractional		
Atom	(2*X*)	(2*Y*)	(2*Z*)	(2*x*)	(12*y*)	(2*z*)
Cu1	0	0	0	0	0	0
	2	0	0	1	2	1
	2	−2	0	0	4	0
	4	−2	0	1	6	1
	4	−4	0	0	8	0
	6	−4	0	1	10	1
Cu2	1	0	−1	0	1	1
	2	−1	1	1	3	0
	3	−2	−1	0	5	1
	4	−3	1	1	7	0
	5	−4	−1	0	9	1
	6	−5	1	1	11	0
Sn	1	1	0	1	0	1
	1	−1	0	0	2	0
	3	−1	0	1	4	1
	3	−3	0	0	6	0
	5	−3	0	1	8	1
	5	−5	0	0	10	0
Zn	1	0	1	1	1	0
	2	−1	−1	0	3	1
	3	−2	1	1	5	0
	4	−3	−1	0	7	1
	5	−4	1	1	9	0
	6	−5	−1	0	11	1

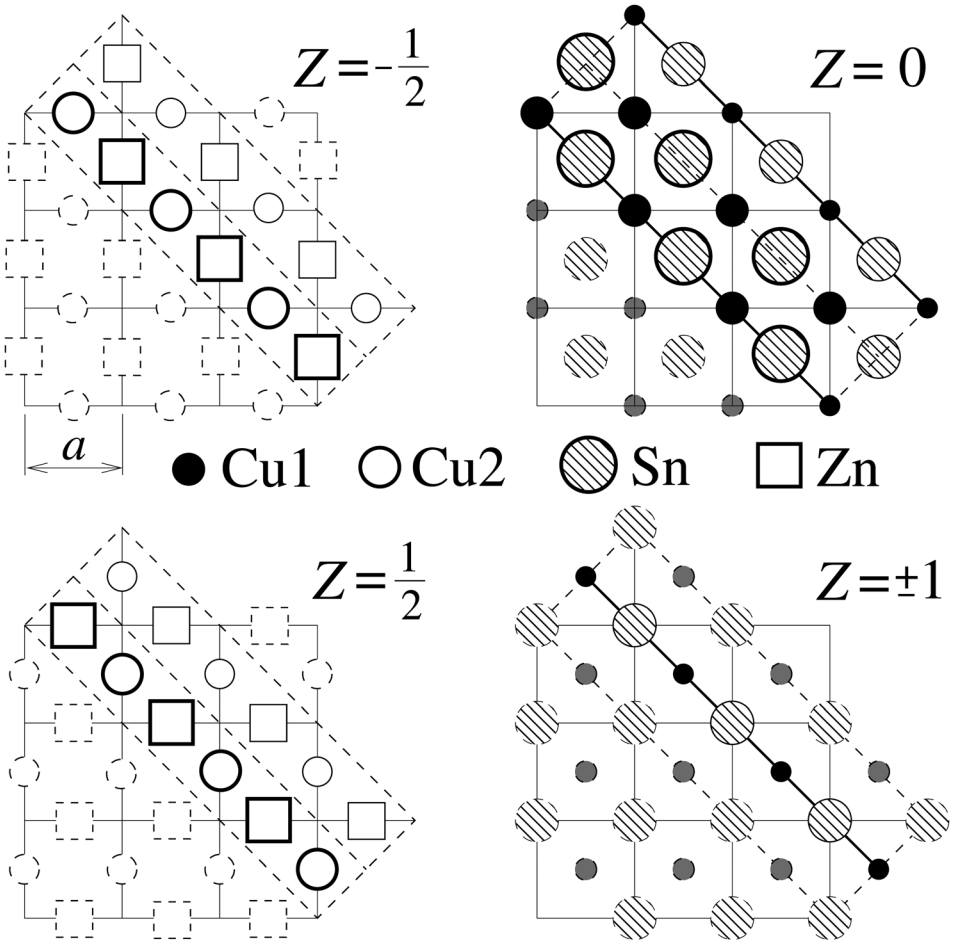

FIG. 8. Monoclinic unit cell (doubly elongated that of CTSe) sliced by several (001) layers of the kesterite structure (only cations are shown). Edges of the unit cell which lie in the corresponding planes are indicated by thick (diagonal) lines; the projection of the rest of the unit cell outline is shown dashed. The nonequivalent atoms (listed also in Table IV) in the unit cell are shown large with thick contours; replicated atoms at the unit cell surface are shown smaller and thinner; the atoms outside the unit cell have dashed contours.

to find its places over the doubled CTSe cell, as summarized in Table IV. Fig. 8 shows the placement of the monoclinic unit cell over the underlying kesterite structure.

The relation between atom coordinates in Cartesian setting (X, Y, Z) with respect to lattice constant a and fractional ones (x, y, z) in units of **A**, **B**, **C** is as follows

$$\begin{pmatrix} X \\ Y \\ Z \end{pmatrix} = \begin{pmatrix} \frac{1}{2} & 3 & \frac{1}{2} \\ \frac{1}{2} & -3 & \frac{1}{2} \\ 1 & 0 & -1 \end{pmatrix} \begin{pmatrix} x \\ y \\ z \end{pmatrix}, \tag{A3}$$

$$\begin{pmatrix} x \\ y \\ z \end{pmatrix} = \begin{pmatrix} \frac{1}{2} & \frac{1}{2} & \frac{1}{2} \\ \frac{1}{6} & -\frac{1}{6} & 0 \\ \frac{1}{2} & \frac{1}{2} & -\frac{1}{2} \end{pmatrix} \begin{pmatrix} X \\ Y \\ Z \end{pmatrix}. \tag{A4}$$

The atomic coordinates of CTSe given in Table III of Delgado *et al.*[11] look very different from those in Table IV—all cation coordinates are far from zero. In fact, the underlying zincblende structure (if no distinction between cations is done), according to Ref. 11, is only slightly distorted (within 2%), but a rigid shift is applied to all coordinates, to satisfy the structure requirements of the space group in question. The "nominal" (undistorted) coordinates in Table III of Delgado *et al.* would read as follows: Cu1 $(\frac{3}{8}\ \frac{1}{4}\ \frac{5}{8})$; Cu2 $(\frac{3}{8}\ \frac{5}{12}\ \frac{1}{8})$; Sn $(\frac{3}{8}\ \frac{1}{12}\ \frac{1}{8})$; Se1 $(0\ \frac{5}{12}\ 0)$; Se2 $(0\ \frac{1}{12}\ 0)$; Se3 $(\frac{1}{2}\ \frac{1}{4}\ 0)$. We recall that these coordinates are relative to "short" (not doubled) monoclinic cell, with $\mathbf{B}' = (\frac{3}{2}\ -\frac{3}{2}\ 0)$, and each site, being of multiplicity 4 as is the only possible in the space group *Cc* (No. 9), expands into four as follows: (x,y,z); $(\frac{1}{2}+x, \frac{1}{2}+y, z)$; $(x, \bar{y}, \frac{1}{2}+z)$; $(\frac{1}{2}+x, \frac{1}{2}-y, \frac{1}{2}+z)$.

In order to identify the rigid shift and relate the atoms in two different settings, we compare the zincblende atomic positions of cations and anions, without discriminating within each of these groups, according to "our" direct counting and to the above positions, expanded according their multiplicities in the *Cc* space group.

Table V gives fractional coordinates, in the units of **A**, **B**′, **C**, of generic cation-anion zincblende. This amounts to taking half of positions from Table IV, namely those with $y < \frac{1}{2}$, and doubling their y-coordinate; moreover, anion positions are added. The latter are added as in the "standard" definition of kesterite[21] with their coordinates in the setting of Table III being close to $(X \approx \frac{3}{4}, Y \approx \frac{3}{4}, Z \approx \frac{3}{4})$ rather than to $(X \approx \frac{3}{4}, Y \approx \frac{3}{4}, Z \approx \frac{1}{4})$. The "mirror symmetric" placement of anions according to the latter choice is equally possible; it will simply result in interchanged x and z coordinates for each atom.

Table VI makes the explicit expansion of "nominal" (undisplaced) coordinates of CTSe over the same unit cell. It is easy to notice that a uniform shift exists, in fact multiple choices thereof that would bring the coordinates of Table V

TABLE V. Atomic coordinates in zincblende structure, expanded over the single monoclinic cell, in units of **A**/8, **B**′/12, **C**/8. The last column indicates the equivalent atom from Table VI obtained by applying translation $(-\frac{1}{8}\ \frac{1}{4}\ \frac{1}{8})$.

	Coordinates			
Atom no.	(8x)	(12y)	(8z)	Equiv. atom in Table VI
		Cations		
1	0	0	0	iv
2	4	0	4	i
3	4	2	0	v
4	0	2	4	xii
5	0	4	0	x
6	4	4	4	vii
7	4	6	0	iii
8	0	6	4	ii
9	0	8	0	vi
10	4	8	4	xi
11	4	10	0	ix
12	0	10	4	viii
		Anions		
13	1	0	3	xxiv
14	5	0	7	xxi
15	1	2	7	xiii
16	5	2	3	xx
17	1	4	3	xv
18	5	4	7	xviii
19	1	6	7	xxii
20	5	6	3	xxiii
21	1	8	3	xix
22	5	8	7	xiv
23	1	10	7	xvii
24	5	10	3	xvi

TABLE VI. Nominal (undistorted) atomic coordinates of monoclinic CTSe, in units of **A**/8, **B**′/12, **C**/8. The last column indicates the equivalent atom from Table V obtained by translation $(\frac{1}{8}\ \frac{1}{12}\ -\frac{1}{8})$.

		Coordinates			
Type	Atom no.	(8x)	(12y)	(8z)	Equiv. atom in Table V
			Cations		
Cu1	i	3	3	5	6
	ii	7	9	5	12
	iii	3	9	1	11
	iv	7	3	1	5
Cu2	v	3	5	1	7
	vi	7	11	1	1
	vii	3	7	5	10
	viii	7	1	5	4
Sn	ix	3	1	1	3
	x	7	7	1	9
	xi	3	11	5	2
	xii	7	5	5	8
			Anions		
Se1	xiii	0	5	0	19
	xiv	4	11	0	14
	xv	0	7	4	21
	xvi	4	1	4	16
Se2	xvii	0	1	0	15
	xviii	4	7	0	22
	xix	0	11	4	13
	xx	4	5	4	20
Se3	xxi	4	3	0	18
	xxii	0	9	0	23
	xxiii	4	9	4	24
	xxiv	0	3	4	17

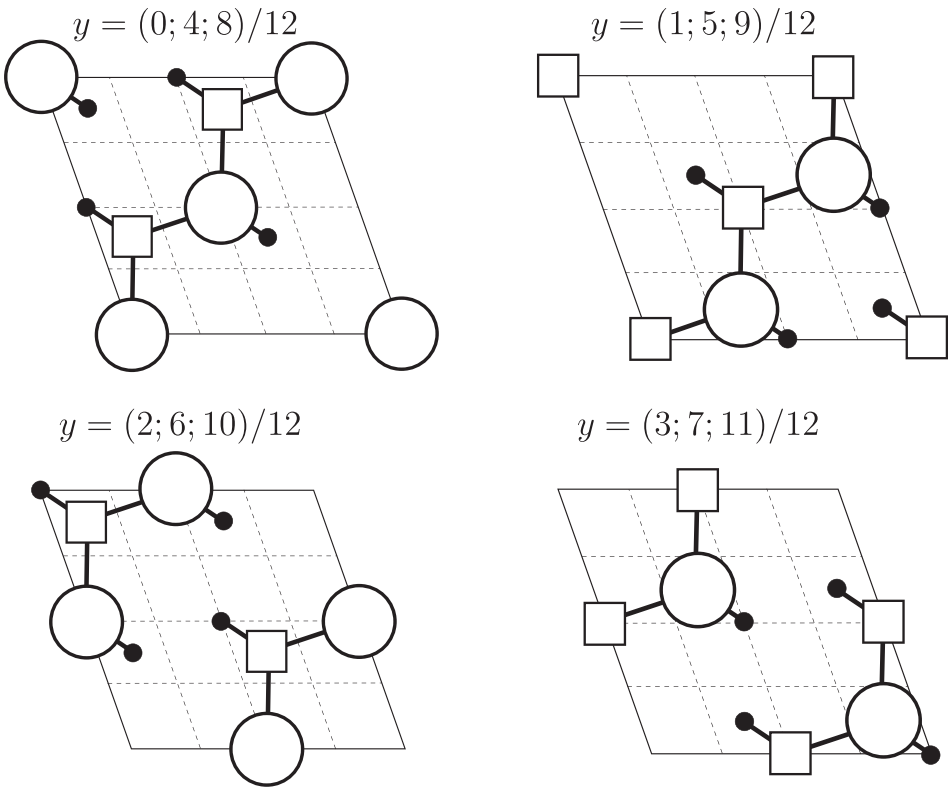

FIG. 9. Placement of atoms in consecutive (010) planes of the monoclinic structure of CTSe. Left column: in the "zincblende" setting, as in Table V. Right column: as in the "native CTSe" setting, as in Table VI. Cations are indicated by white circles, anions by squares. Thick points mark (x,y) projections of atoms situated in the adjacent planes below and above.

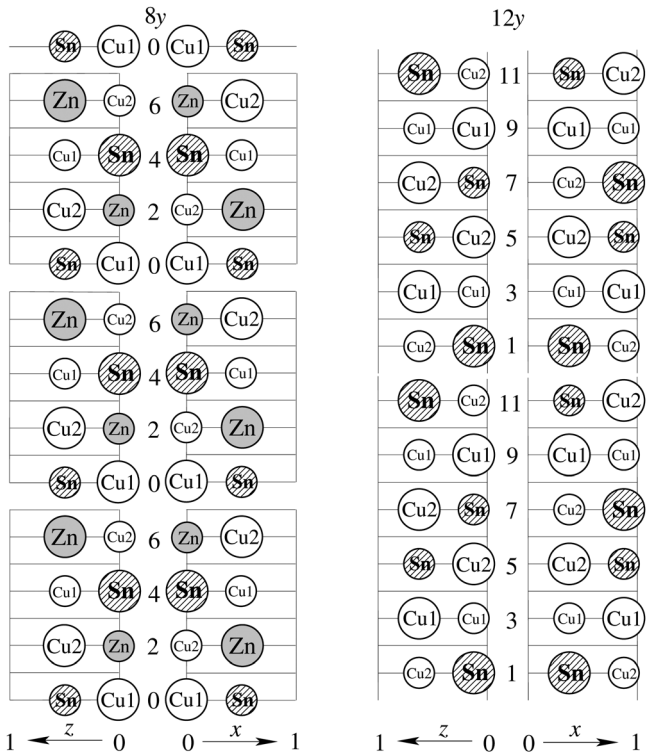

FIG. 10. Commensurate sequence of (010) planes, in the common monoclinic setting, of CZTSe kesterite (left, three unit cells along [010]) and CTSe (right, two unit cells). Only cations are shown in their projections on the (x,y) and (z,y) planes. The size of circle roughly indicates whether the atom is close (large circles) or far (small circles) from the projection plane. See Fig. 9 for the (x,z) projections.

into those of Table VI. An example of such attribution, for two different translations, is indicated in the last column of each table.

The "necessity" of the shift is imposed by symmetry operations of the *Cc* group which permute four atoms within each species. In a calculation which does not make use of crystal symmetry, as our present one, this shift has no effect whatsoever. We note that the alternative "mirror" choice of anionic positions in kesterite would merely lead to different choice of the uniform shift vector.

More generally, each of two settings is a stacking of alternating (010) cation-anion planes, as shown in Fig. 9. Each plane is connected to adjacent ones, forming zigzag (planar) cation-anion chains along [010]; perpendicular "flat" similar chains run in the planes, along [101]. One can see that, other than by introducing a rigid shift, the two settings are related by cation $\leftrightarrow$ anion interchange, accompanied by $x \leftrightarrow z$ swap, in one of the settings.

We restore now the non-equivalence of cations, recalling that they can belong to three chemical species, as in CZTSe kesterite. A remarkable feature of atom mapping shown by Tables IV and V, confirmed also by Fig. 10, is that the mapping of a given species inevitably occurs into *all* cation species of the counterpart structure. That is, it is impossible to pinpoint Sn, or Cu, of CZTSe to their native positions in CTSe and let, say, Zn atom to appear at whatever cation sites remain vacant. Instead, the substitution pattern is nodular, along [010]: tripled unit cell of kesterite is commensurate with double unit cell of CTSe. In the sequence of (010) planes we find Cu-Se ones, common for both structures; moreover, the CZSe structure contains Cu-Cu planes, and kesterite—Cu-Zn ones. Looking at chains that go along [010] and hold the planes together, we notice that Sn enters only "isolated" between two Zn atoms in CZTSe, whereas CTSe contains Sn "pairs". Such similarities and differences find their manifestation in the vibration spectra of both systems.

[1]L. M. Peter, Philos. Trans. R. Soc. London, Ser. A **369**, 1840 (2011).
[2]T. K. Todorov, K. B. Reuter, and D. B. Mitzi, Adv. Mater. **22**, E156 (2010).
[3]S. Chen, X. G. Gong, A. Walsh, and S.-H. Wei, Appl. Phys. Lett. **94**, 041903 (2009).
[4]P. A. Fernandes, P. M. P. Salomé, and A. F. da Cunha, J. Phys. D: Appl. Phys. **43**, 215403 (2010).
[5]T. Maeda, S. Nakamura, and T. Wada, Thin Solid Films **519**, 7513 (2011).
[6]M. Ganchev, J. Iljina, L. Kaupmees, T. Raadik, O. Volobujeva, A. Mere, M. Altosaar, J. Raudoja, and E. Mellikov, Thin Solid Films **519**, 7394 (2011).
[7]O. Pagès, A. V. Postnikov, M. Kassem, A. Chafi, A. Nassour, and S. Doyen, Phys. Rev. B **77**, 125208 (2008).
[8]A. V. Postnikov, O. Pagès, and J. Hugel, Phys. Rev. B **71**, 115206 (2005).
[9]G. Marcano, C. Rincón, L. M. de Chalbaud, D. B. Bracho, and G. Sánchez Pérez, J. Appl. Phys. **90**, 1847 (2001).
[10]G. Marcano, L. M. de Chalbaud, C. Rincón, and G. Sánchez Pérez, Mater. Lett. **53**, 151 (2002).
[11]G. E. Delgado, A. J. Mora, G. Marcano, and C. Rincón, Mater. Res. Bull. **38**, 1949 (2003).
[12]See http://www.icmab.es/siesta/ for Siesta homepage.
[13]P. Ordejón, E. Artacho, and J. M. Soler, Phys. Rev. B **53**, R10441 (1996).
[14]J. M. Soler, E. Artacho, J. D. Gale, A. García, J. Junquera, P. Ordejón, and D. Sánchez-Portal, J. Phys.: Condens. Matter **14**, 2745 (2002).
[15]N. Troullier and J. L. Martins, Phys. Rev. B **43**, 1993 (1991).
[16]N. B. Mortazavi Amiri and A. Postnikov, Phys. Rev. B **82**, 205204 (2010).
[17]Y.-T. Zhai, S. Chen, J.-H. Yang, H.-J. Xiang, X.-G. Gong, A. Walsh, J. Kang, and S.-H. Wei, Phys. Rev. B **84**, 075213 (2011).
[18]M. Altosaar, J. Raudoja, K. Timmo, M. Danilson, M. Grossberg, J. Krustok, and E. Mellikov, Phys. Status Solidi A **205**, 167 (2008).
[19]M. Grossberg, J. Krustok, K. Timmo, and M. Altosaar, Thin Solid Films **517**, 2489 (2009).
[20]G. Marcano, C. Rincón, S. A. López, G. Sánchez Pérez, J. L. Herrera-Pérez, J. G. Mendoza-Alvarez, and P. Rodríguez, Solid State Commun. **151**, 84 (2011).
[21]S. R. Hall, J. T. Szymanski, and J. M. Stewart, Can. Mineral. **16**, 131 (1978).